PHYSICS LETTERS B

Polarized parton distributions at an electron–ion collider

CrossMark

NNPDF Collaboration

Richard D. Ball [a], Stefano Forte [b,*], Alberto Guffanti [c], Emanuele R. Nocera [b], Giovanni Ridolfi [d], Juan Rojo [e]

[a] *Tait Institute, University of Edinburgh, JCMB, KB, Mayfield Rd, Edinburgh EH9 3JZ, Scotland, United Kingdom*
[b] *Dipartimento di Fisica, Università di Milano and INFN, Sezione di Milano, Via Celoria 16, I-20133 Milano, Italy*
[c] *The Niels Bohr International Academy and Discovery Center, The Niels Bohr Institute, Blegdamsvej 17, DK-2100 Copenhagen, Denmark*
[d] *Dipartimento di Fisica, Università di Genova and INFN, Sezione di Genova, Genova, Italy*
[e] *PH Department, TH Unit, CERN, CH-1211 Geneva 23, Switzerland*

A R T I C L E   I N F O

A B S T R A C T

We study the potential impact of inclusive deep-inelastic scattering data from a future electron–ion collider (EIC) on longitudinally polarized parton distributions (PDFs). We perform a PDF determination using the NNPDF methodology, based on sets of deep-inelastic EIC pseudodata, for different realistic choices of the electron and proton beam energies. We compare the results to our current polarized PDF set, NNPDFpol1.0, based on a fit to fixed-target inclusive DIS data. We show that the uncertainties on the first moments of the polarized quark singlet and gluon distributions are substantially reduced in comparison to NNPDFpol1.0, but also that more measurements may be needed to ultimately pin down the size of the gluon contribution to the nucleon spin.

© 2013 The Authors. Published by Elsevier B.V. Open access under CC BY license.

The accurate determination of polarized parton distribution functions (PDFs), along with a reliable estimate of their uncertainties, has been the goal of several recent studies [1–5]. In Ref. [5] we presented a first determination of polarized PDFs based on the NNPDF methodology [5], NNPDFpol1.0, which uses Monte Carlo sampling for error propagation and unbiased PDF parametrization in terms of neural networks. The bulk of experimental information on longitudinally polarized proton structure comes from inclusive neutral-current deep-inelastic scattering (DIS), which allows one to obtain information on the light quark–antiquark combinations $\Delta u + \Delta \bar{u}$, $\Delta d + \Delta \bar{d}$, $\Delta s + \Delta \bar{s}$ and on the gluon distribution Δg. However, DIS data covers only a small kinematic region of momentum fractions and energies (x, Q^2). On the one hand, the lack of experimental information for $x \lesssim 10^{-3}$ prevents a reliable determination of polarized PDFs at small-x. Hence, their first moments will strongly depend on the functional form one assumes for PDF extrapolation to the unmeasured x region [1]. On the other hand, the gluon PDF, which is determined by scaling violations, is only

weakly constrained, due to the small lever-arm in Q^2 of the experimental data.

For these reasons, despite many efforts, both experimental and theoretical, the size of the polarized gluon contribution to the nucleon spin is still largely uncertain [5,6]. Open charm photoproduction data from COMPASS [7] do not change this state of affairs: they were shown in Ref. [8] to have almost no impact on Δg. Present and future polarized hadron collider measurements from RHIC [9–13], specifically semi-inclusive particle production and jet data, should provide further constraints on Δg, but restricted to the medium- and large-x region.

An Electron–Ion Collider (EIC) [14–16], with polarized lepton and hadron beams, would allow for a widening of the kinematic region comparable to the one achieved in the unpolarized case with the DESY–HERA experiments H1 and ZEUS [17] (note that a Large Hadron–electron Collider (LHeC) [18] would not have the option of polarizing the hadron beam). The potential impact of the EIC on the knowledge of the nucleon spin has been quantitatively assessed in a recent study [19], in which projected neutral-current inclusive DIS and semi-inclusive DIS (SIDIS) artificial data were added to the DSSV polarized PDF determination [6]; this study was then extended by also providing an estimate of the impact of charged-current inclusive DIS pseudo-data on the polarized quark flavor separation in Ref. [20]. In view of the fact that a substantially larger gluon uncertainty was found in Ref. [5] in comparison to previous PDF determinations [1–4], it is worth repeating the study

---

Table 1

The three EIC pseudodata sets [19]. For each set we show the number of points N_{dat}, the electron and proton beam energies E_e and E_p, the center-of-mass energy $\sqrt{s}$, the kinematic coverage in the momentum fraction x, and the average absolute statistical uncertainty $\langle \delta g_1 \rangle$.

| Experiment	Set	N_{dat}	$E_e \times E_p$ [GeV]	$\sqrt{s}$ [GeV]	x_{min}	x_{max}	$\langle \delta g_1 \rangle$
EIC	EIC-G1P-1	56	5×100	44.7	8.2×10^{-4}	0.51	0.010
	EIC-G1P-2	63	5×250	70.7	3.2×10^{-4}	0.51	0.032
	EIC-G1P-3	61	20×250	141	8.2×10^{-5}	0.32	0.042

of the impact of EIC data, but now using NNPDF methodology. This is the goal of the present Letter.

Two alternative designs have been proposed for the EIC so far: the electron Relativistic Heavy Ion Collider (eRHIC) at Brookhaven National Laboratory (BNL) [21] and the Electron Light Ion Collider (ELIC) at Jefferson Laboratory (JLab) [22]. In both cases, a staged upgrade of the existing facilities has been planned [14–16], so that an increased center-of-mass energy would be available at each stage. Concerning the eRHIC option of an EIC [21], first measurements would be taken by colliding the present RHIC proton beam of energy $E_p = 100$–250 GeV with an electron beam of energy $E_e = 5$ GeV, while a later stage envisages electron beams with energy up to $E_e = 20$ GeV.

In order to quantitatively assess the impact of the EIC data, we have supplemented our previous QCD analysis [5] with DIS pseudodata from Ref. [19], which consist of three sets of data points at different possible eRHIC electron and proton beam energies, as discussed above. These pseudodata were produced by running the PEPSI Monte Carlo (MC) generator [23], assuming momentum transfer $Q^2 > 1$ GeV^2, squared invariant mass of the virtual photon–proton system $W^2 > 10$ GeV^2 and fractional energy of the virtual photon $0.01 \leqslant y \leqslant 0.95$; they are provided in five (four) bins per logarithmic decade in x (Q^2). For each dataset, the Q^2 range spans the values from $Q^2_{min} = 1.39$ GeV^2 to $Q^2_{max} = 781.2$ GeV^2, while the accessible values of momentum fraction $x = Q^2/(sy)$ depend on the available center-of-mass energy, $\sqrt{s}$. In Table 1, we summarize, for each data set, the number of pseudodata N_{dat}; the electron and proton beam energies E_e, E_p; the corresponding center-of-mass energies $\sqrt{s}$; and the smallest and largest accessible value in the momentum fraction range, x_{min} and x_{max} respectively.

The kinematic coverage of the EIC pseudodata is displayed in Fig. 1 together with the fixed-target DIS data points included in our previous analysis [5]. The dashed regions show the overall kinematic reach of the EIC data with the two electron beam energies $E_e = 5$ GeV or $E_e = 20$ GeV, corresponding to each of the two stages at eRHIC. It is apparent from Fig. 1 that EIC data will extend the kinematic coverage significantly, even for the lowest center-of-mass energy. In particular, hitherto unreachable small x values, down to 10^{-4}, will be attained, thereby leading to a significant reduction of the uncertainty in the low-x extrapolation region. Furthermore, the increased lever-arm in Q^2, for almost all values of x, should allow for much more stringent constraints on $\Delta g(x, Q^2)$ from scaling violations.

The observable provided in Ref. [19] for inclusive DIS pseudodata is the ratio $g_1(x, Q^2)/F_1(x, Q^2)$; we refer the reader to Ref. [5] for a discussion of its relation to experimentally measured asymmetries. The generation of pseudodata assumes a "true" underlying set of parton distributions. In Ref. [19] these are taken to be DSSV+ [6] and MRST [24] polarized and unpolarized PDFs respectively. Uncertainties are then determined assuming an integrated luminosity of 10 fb^{-1}, which corresponds to a few months operations for the anticipated luminosities for eRHIC [21], and a 70% beam polarization. Because the DSSV+ polarized gluon has rather more structure than that of NNPDFpol1.0, which is largely compatible with zero, assuming this input shape will allow us to
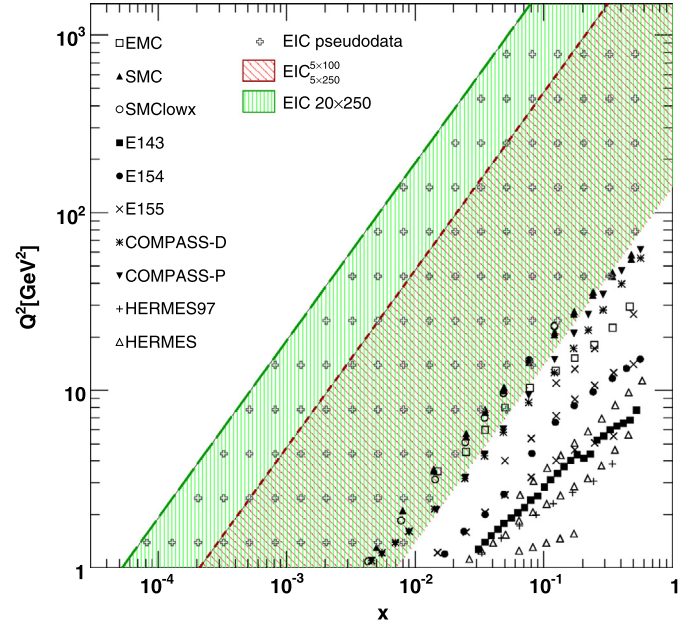

Fig. 1. Kinematic coverage in the (x, Q^2) plane for the fixed-target experimental data included in the NNPDFpol1.0 polarized parton fit [5] and the EIC pseudodata from [19]. The shaded bands show the expected kinematic reach of each of the two EIC scenarios discussed in the text.

test whether the EIC data are sufficiently accurate to determine the shape of the gluon distribution.

We reconstruct the g_1 polarized structure function from the pseudodata following the same procedure used in Ref. [5] for the E155 experiment. We provide its average statistical uncertainty in the last column of Table 1. A comparison of these values with the analogous quantities for fixed-target experiments (see Table 2 in Ref. [5]) clearly shows that EIC data are expected to be far more precise, with uncertainties reduced up to one order of magnitude. No information on the expected systematic uncertainties is available. We will perform two different fits, corresponding to the two stages envisaged for the eRHIC option of an EIC [21] discussed above, which will be referred to as NNPDFpolEIC-A and NNPDFpolEIC-B. The former includes the first two sets of pseudodata listed in Table 1, while the latter also includes the third set.

The methodology for the determination of PDFs follows the one adopted in Ref. [5], to which we refer for details. The only modifications are the following. First, we have re-tuned the genetic algorithm which is used for minimization, and the parameters which determine its stopping at the optimal fit. This is required to obtain a good fit quality with EIC pseudodata, which are very accurate in comparison to their fixed-target counterparts and cover a wider kinematic region (see Fig. 1). In particular, we have used a larger population of mutants, increased the number of weighted training generations and tuned the stopping parameters. Furthermore, we have redetermined the range in which preprocessing exponents are randomized, since the new information from EIC pseudodata may modify the large- and small-x PDF behavior. In Table 2, we show

Distribution of $\chi_{\text{tot}}^{2(k)}$ for individual sets
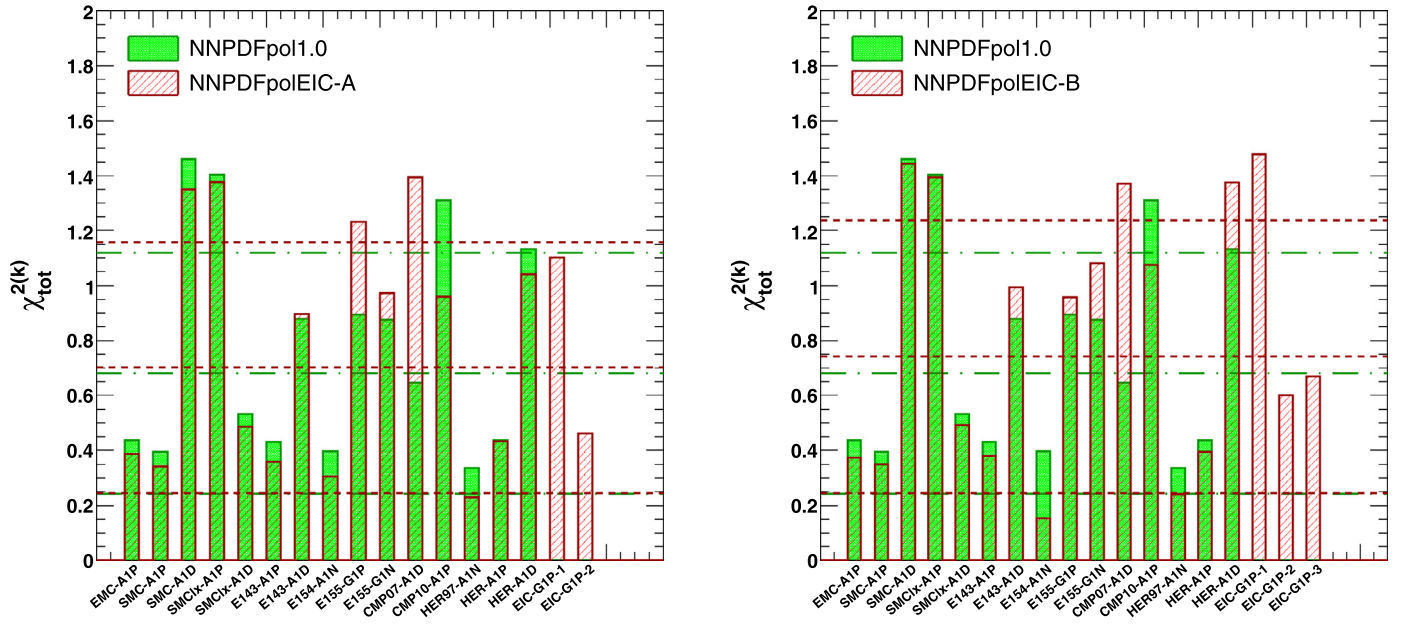
Fig. 2. Value of the χ^2 per data point for the datasets included in the `NNPDFpolEIC-A` (left) and in the `NNPDFpolEIC-B` (right) fits, compared to `NNPDFpol1.0` [5]. The horizontal lines correspond to the unweighted average of the χ^2 values shown, and the one-sigma interval about it. The dashed lines refer to `NNPDFpolEIC-A` (left plot) or `NNPDFpolEIC-B` (right plot) fits, while the dot-dashed lines refer to `NNPDFpol1.0` [5].

Table 2

Ranges for the small- and large-x preprocessing exponents.

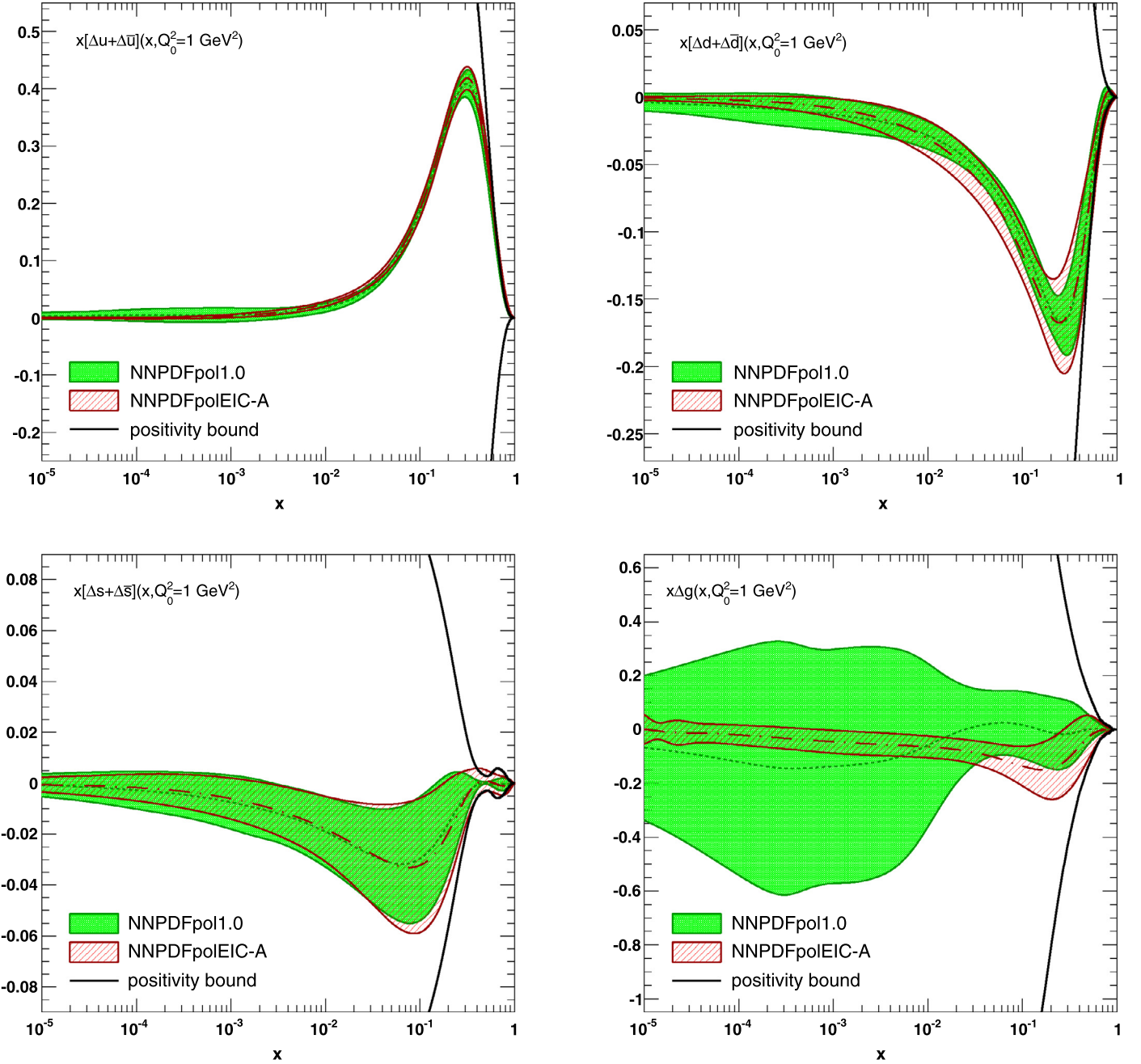| PDF	NNPDFpol1.0 [5]		NNPDFpolEIC	
	m	n	m	n
$\Delta\Sigma(x, Q_0^2)$	[1.5, 3.5]	[0.2, 0.7]	[1.5, 3.5]	[0.1, 0.7]
$\Delta g(x, Q_0^2)$	[2.5, 5.0]	[0.4, 0.9]	[2.0, 4.0]	[0.1, 0.8]
$\Delta T_3(x, Q_0^2)$	[1.5, 3.5]	[0.4, 0.7]	[1.5, 3.0]	[0.1, 0.6]
$\Delta T_8(x, Q_0^2)$	[1.5, 3.0]	[0.1, 0.6]	[1.5, 3.0]	[0.1, 0.6]

Table 3

Statistical estimators and average training length for the `NNPDFpolEIC-A` and `NNPDFpolEIC-B` with $N_{\text{rep}} = 100$ replicas, compared to the `NNPDFpol1.0` reference fit [5].

	NNPDFpol1.0 [5]	NNPDFpolEIC-A	NNPDFpolEIC-B
χ_{tot}^2	0.77	0.79	0.86
$\langle E \rangle \pm \sigma_E$	1.82 ± 0.18	2.24 ± 0.34	2.44 ± 0.31
$\langle E_{\text{tr}} \rangle \pm \sigma_{E_{\text{tr}}}$	1.66 ± 0.49	1.87 ± 0.54	1.81 ± 0.79
$\langle E_{\text{val}} \rangle \pm \sigma_{E_{\text{val}}}$	1.88 ± 0.67	2.61 ± 1.05	2.47 ± 1.17
$\langle \chi^{2(k)} \rangle \pm \sigma_{\chi^2}$	0.91 ± 0.12	1.30 ± 0.31	1.50 ± 0.30
$\langle TL \rangle \pm \sigma_{\text{TL}}$	6927 ± 3839	7467 ± 3678	19 320 ± 14 625

the values we use for the present fit, compared to `NNPDFpol1.0`. We have checked that our choice of preprocessing exponents does not bias our fit, according to the procedure discussed in Section 4.1 of Ref. [5].

Various general features of the `NNPDFpolEIC-A` and `NNPDFpolEIC-B` PDF determinations are summarized in Table 3, compared to `NNPDFpol1.0`. These include the χ^2 per data point of the final best-fit PDF compared to data, (denoted as χ_{tot}^2), the average and standard deviation over the replica sample of the same figure of merit for each PDF replica when compared to the corresponding data replica (denoted as $\langle E \rangle \pm \sigma_E$ computed for the total, training and validation sets, the average and standard deviation of the χ^2 of each replica when compared to data (denoted as $\langle \chi^{2(k)} \rangle$), and the average number of iterations of the genetic algorithm at stopping $\langle TL \rangle$ and its standard deviation over the replica sample. A more detailed discussion of these quantities can be found in previous NNPDF papers, in particular in Refs. [25,26], and Ref. [5] for the polarized case.

The fit quality, as measured by χ_{tot}^2, is comparable to that of `NNPDFpol1.0` ($\chi_{\text{tot}}^2 = 0.77$) for both the `NNPDFpolEIC-A` ($\chi_{\text{tot}}^2 = 0.79$) and the `NNPDFpolEIC-B` ($\chi_{\text{tot}}^2 = 0.86$) fits. This shows that our fitting procedure can easily accommodate EIC pseudodata. The histogram of χ^2 values for each data set included in our fits is shown in Fig. 2, together with the `NNPDFpol1.0` [5] result; the unweighted average $\langle \chi^2 \rangle_{\text{set}} \equiv \frac{1}{N_{\text{set}}} \sum_{j=1}^{N_{\text{set}}} \chi_{\text{set},j}^2$ and standard deviation over data sets are also shown. As already pointed out in Ref. [5], χ^2 values significantly below one are found as

a consequence of the fact that information on correlated systematics is not available for most experiments, and thus statistical and systematic errors are added in quadrature. Note that this is not the case for the EIC pseudodata, for which, as mentioned, no systematic uncertainty was included; this may explain the somewhat larger (closer to one) value of the χ^2 per data point which is found when the pseudodata are included.

We notice that EIC pseudodata, which are expected to be rather more precise than fixed-target DIS experimental data, require more training to be properly learned by the neural network. This is apparent in the increase in $\langle TL \rangle$ in Table 3 when going from `NNPDFpol1.0` to `NNPDFpolEIC-A` and then `NNPDFpolEIC-B`. We checked that the statistical features discussed above do not improve if we run very long fits, up to $N_{\text{gen}}^{\text{max}} = 50000$ generations, without dynamical stopping. In particular we do not observe a decrease of the χ^2 for those experiments whose value exceeds the average by more than one sigma. This ensures that these deviations are not due to underlearning, i.e. insufficiently long minimization.

Parton distributions from the `NNPDFpolEIC-A` and `NNPDFpolEIC-B` fits are compared to `NNPDFpol1.0` [5] in Figs. 3 and 4 respectively. In these plots, PDFs are displayed at $Q_0^2 = 1$ GeV^2 as a function of x on a logarithmic scale; all uncertainties shown here are one-σ bands. The positivity bound, obtained from the

Fig. 3. The `NNPDFpolEIC-A` parton distributions at $Q_0^2 = 1$ GeV^2 plotted as a function of x on a logarithmic scale, compared to `NNPDFpol1.0` [5].

`NNPDF2.3` NLO unpolarized set [27] as discussed in Ref. [5], is also drawn.

The most visible impact of inclusive EIC pseudodata in both our fits is the reduction of PDF uncertainties in the low-x region ($x \lesssim 10^{-3}$) for light flavors and the gluon. The size of the effects is different for different PDFs. As expected, the most dramatic improvement is seen for the gluon, while uncertainties on light quarks are only reduced by a significant factor in the small x region. The uncertainty on the strange distribution is essentially unaffected: unlike in Ref. [19], we find no improvement on strangeness, due to the fact that we do not include semi-inclusive kaon production data, contrary to what was done there. When moving from `NNPDFpolEIC-A` to `NNPDFpolEIC-B` the gluon uncertainty decreases further, while other PDF uncertainties are basically unchanged.

In Fig. 5 we compare the polarized gluon PDF in our EIC fits to the DSSV [1] and `NNPDFpol1.0` [5] parton determinations, both at $Q_0^2 = 1$ GeV^2 and $Q^2 = 10$ GeV^2. The DSSV uncertainty is the Hessian uncertainty computed assuming $\Delta \chi^2 = 1$, which corresponds to the default uncertainty estimate in Ref. [1]. This choice may lead to somewhat underestimated uncertainties: indeed, a more conservative uncertainty estimate is also provided in Ref. [1]. Furthermore, it is known from unpolarized global PDF fits that a somewhat larger 'tolerance' T value $\Delta \chi^2 = T$ [28] should be adopted in order for the distribution of χ^2 values between different experiments in the global fit to be reasonable (indeed this choice was made in the polarized fit of Ref. [3], with $T = 12.65$).

It is clear that the gluon PDF from our fits including EIC pseudodata is approaching the DSSV PDF shape, especially at a lower scale where the DSSV gluon does have some structure, despite the
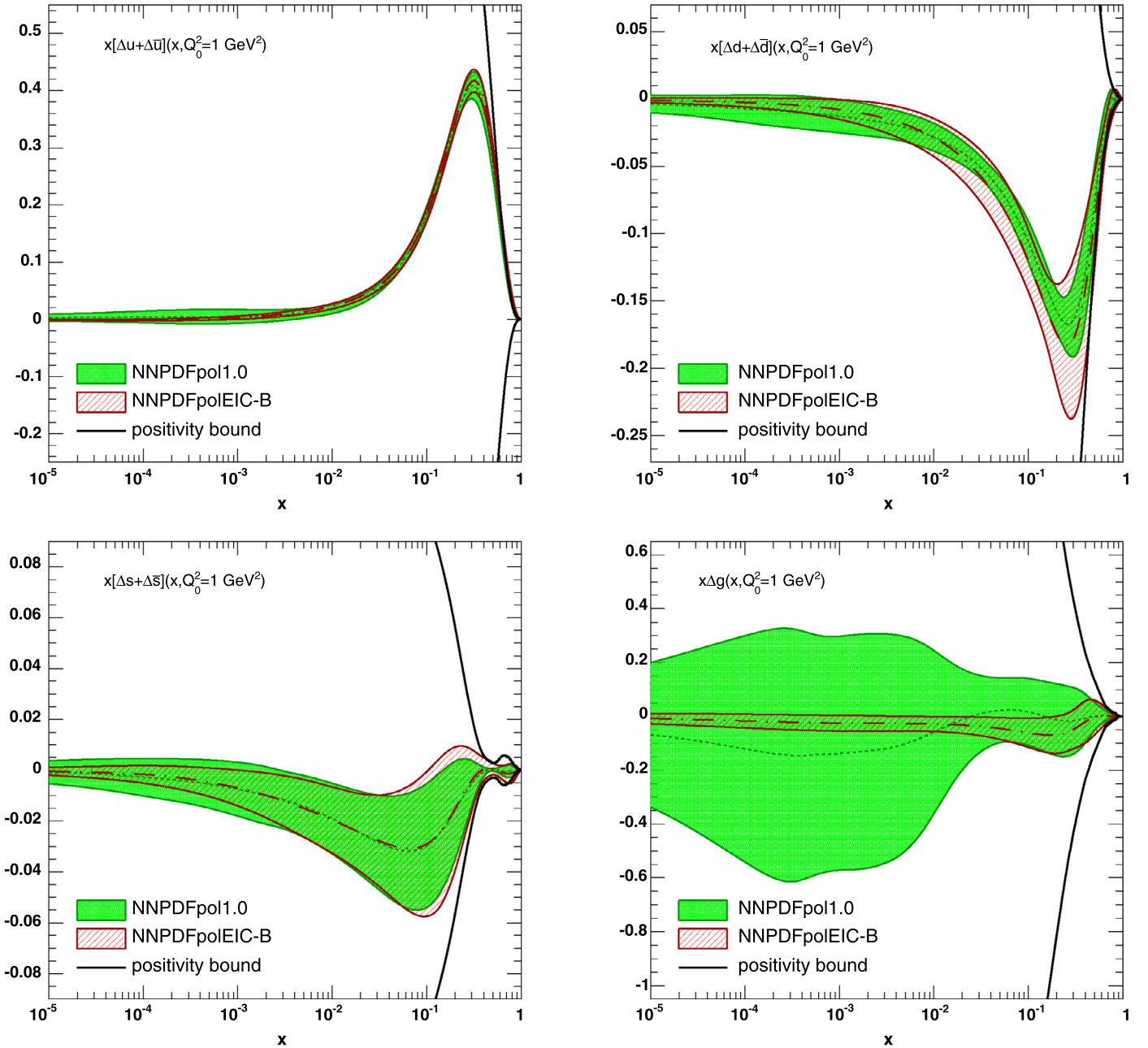
Fig. 4. Same as Fig. 3, but for `NNPDFpolEIC-B`, compared to `NNPDFpol1.0` [5].

fact that at higher scales, where much of the data is located, per-
turbative evolution tends to wash out this shape. Also, this is more
pronounced as more EIC pseudodata are included in our fit, *i.e.*
moving from `NNPDFpolEIC-A` to `NNPDFpolEIC-B`. This means
that EIC data would be sufficiently accurate to reveal the polarized
gluon structure, if any.

It is particularly interesting to examine how the EIC data affect
the determination of the first moments

$$\langle \Delta f(Q^2) \rangle \equiv \int_0^1 dx \, \Delta f(x, Q^2) \tag{1}$$

of the polarized PDFs $\Delta f(x, Q^2)$, as they are directly related to
the nucleon spin structure. We have computed the first moments,
Eq. (1), of the singlet, lightest quark–antiquark combinations and

gluon for the `NNPDFpolEIC-A` and `NNPDFpolEIC-B` PDF sets.
The corresponding central values and one-σ uncertainties at $Q_0^2 =$
1 GeV^2 are shown in Table 4, compared to `NNPDFpol1.0` [5].

It is clear that EIC pseudodata reduce all uncertainties sig-
nificantly. Note that moving from `NNPDFpolEIC-A` to `NNPDF-`
`polEIC-B` does not improve significantly the uncertainty on
quark–antiquark first moments, but it reduces the uncertainty on
the gluon first moment by a factor two. However, it is worth notic-
ing that, despite a reduction of the uncertainty on the gluon first
moment, even for the most accurate `NNPDFpolEIC-B` fit, the
value remains compatible with zero even though the central value
is sizable (and negative).

In order to assess the residual extrapolation uncertainty on the
singlet and gluon first moments, we determine the contribution to
them from the data range $x \in [10^{-3}, 1]$, *i.e.*
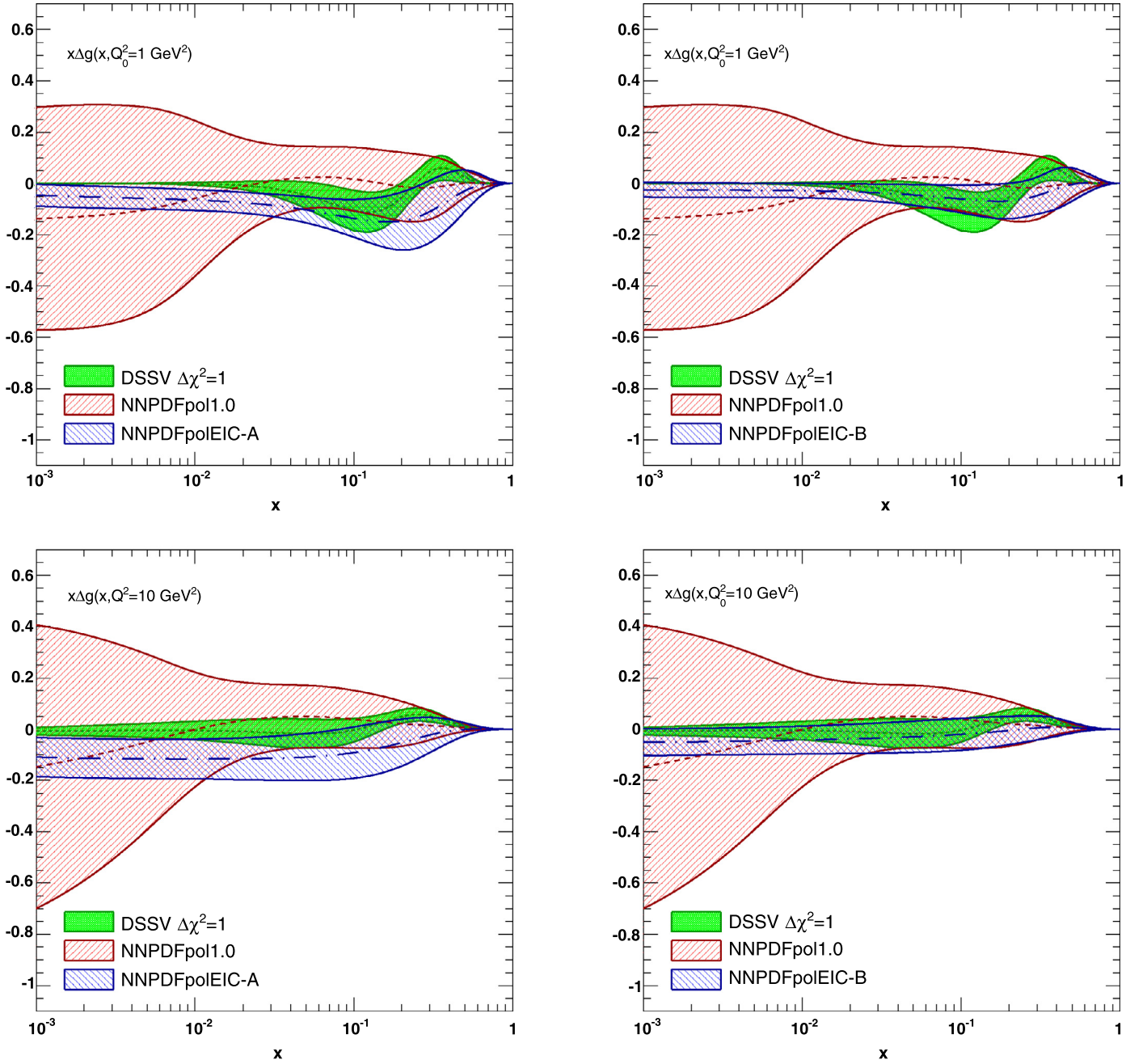
Fig. 5. The polarized gluon PDF $\Delta g(x, Q_0^2)$, at $Q_0^2 = 1$ GeV^2 (upper panels) and at $Q^2 = 10$ GeV^2 (lower panels), in the `NNPDFpolEIC` PDF sets, compared to DSSV [1] and to `NNPDFpol1.0` [5].

$$\langle \Delta\Sigma(Q^2)\rangle_{\mathrm{TR}} \equiv \int_{10^{-3}}^{1} dx \, \Delta\Sigma(x, Q^2),$$

$$\langle \Delta g(Q^2)\rangle_{\mathrm{TR}} \equiv \int_{10^{-3}}^{1} dx \, \Delta g(x, Q^2). \qquad (2)$$

The first moments in Eq. (2) are given in Table 5 at $Q_0^2 = 1$ GeV^2 and $Q^2 = 10$ GeV^2, where results for central values, uncertainties, and correlation coefficients between the gluon and quark are collected.

Comparing the results at $Q^2 = 1$ GeV^2 of Table 4 and Table 5 we see that in the `NNPDFpol1.0` PDF determination for the quark singlet combination the uncertainty on the full first moment is about twice as large as that from the measured region, and for the gluon it is about four times as large. The difference is due to the extra uncertainty coming from the extrapolation. In `NNPDFpolEIC-B` the corresponding increases are by 20% for the quark and 30% for the gluon, which shows that thanks to EIC data the extrapolation uncertainties would be largely under control. The correlation coefficient ρ significantly decreases upon inclusion of the EIC data: this means that the extra information contained in these data allows for an independent determination of the quark and gluon first moments.

In Fig. 6, we plot the one-σ confidence region in the $(\langle\Delta\Sigma(Q^2)\rangle_{\mathrm{TR}}, \langle\Delta g(Q^2)\rangle_{\mathrm{TR}})$ plane at $Q^2 = 10$ GeV^2, for `NNPDFpolEIC-A`, `NNPDFpolEIC-B` and `NNPDFpol1.0` [5]. The main

Table 4

First moments of the polarized quark distributions at $Q_0^2 = 1$ GeV^2 for the fits in the present analysis, compared to `NNPDFpol1.0` [5].

Fit	$\langle \Delta \Sigma \rangle$	$\langle \Delta u + \Delta \bar{u} \rangle$	$\langle \Delta d + \Delta \bar{d} \rangle$	$\langle \Delta s + \Delta \bar{s} \rangle$	$\langle \Delta g \rangle$
`NNPDFpol1.0` [5]	0.22 ± 0.20	0.80 ± 0.08	-0.46 ± 0.08	-0.13 ± 0.10	-1.15 ± 4.19
`NNPDFpolEIC-A`	0.24 ± 0.08	0.82 ± 0.02	-0.45 ± 0.02	-0.13 ± 0.07	-0.59 ± 0.86
`NNPDFpolEIC-B`	0.21 ± 0.06	0.81 ± 0.02	-0.47 ± 0.02	-0.12 ± 0.07	-0.33 ± 0.43

Table 5

The singlet and gluon truncated first moments and their one-σ uncertainties at $Q^2 = 1$ GeV^2 and $Q^2 = 10$ GeV^2 for the `NNPDFpolEIC` PDF sets, compared to `NNPDFpol1.0` [5]. The correlation coefficient ρ at $Q^2 = 10$ GeV^2 is also provided.

	$Q^2 = 1$ GeV^2		$Q^2 = 10$ GeV^2		
	$\langle \Delta \Sigma(Q^2) \rangle_{TR}$	$\langle \Delta g(Q^2) \rangle_{TR}$	$\langle \Delta \Sigma(Q^2) \rangle_{TR}$	$\langle \Delta g(Q^2) \rangle_{TR}$	$\rho(Q^2)$
`NNPDFpol1.0` [5]	0.25 ± 0.09	-0.26 ± 1.19	0.23 ± 0.16	-0.06 ± 1.12	$+0.861$
`NNPDFpolEIC-A`	0.27 ± 0.06	-0.53 ± 0.37	0.23 ± 0.05	-0.59 ± 0.50	-0.186
`NNPDFpolEIC-B`	0.24 ± 0.05	-0.23 ± 0.25	0.22 ± 0.04	-0.19 ± 0.32	-0.103
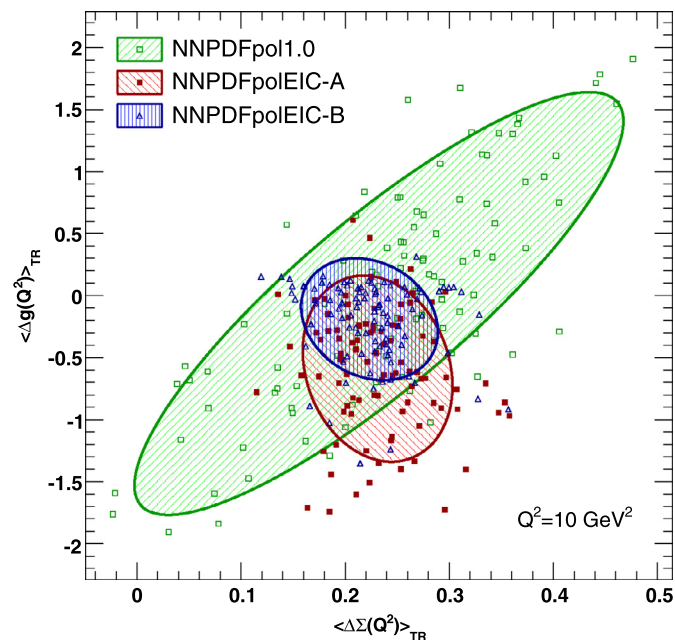
Fig. 6. One-σ confidence region for the quark singlet and gluon first moments in the measured region, Eq. (2). The values for individual replicas are also shown.

result of our analysis, Fig. 6, can be directly compared to Fig. 8 of Ref. [19], which was based on the DSSV fit and is comparable to our `NNPDFpolEIC-B` results. In both analyses EIC pseudodata determine the singlet first moment in the measured region with an uncertainty of about ± 0.05.

On the other hand, in Ref. [19] the uncertainty on the gluon was found to be about ± 0.02, while we get a much larger result of ± 0.30. One may wonder whether this difference may be due at least in part to the fact that the DSSV fit on which the result of Ref. [19] is based also includes jet production and pion production data from RHIC, which may reduce the gluon uncertainty. To answer this, we have computed the contribution to the gluon first moment (again at $Q^2 = 10$ GeV^2) from the reduced region $0.05 \leqslant x \leqslant 0.2$, where the RHIC data are located. We find that the uncertainty on the contribution to the gluon first moment in this restricted range is ± 0.083 using `NNPDFpolEIC-B`, while it is ± 0.147 with `NNPDFpol1.0` and $^{+0.129}_{-0.164}$ with DSSV [29]. We conclude that before the EIC data are added, the uncertainties in `NNPDFpol1.0` and DSSV are quite similar despite the fact that DSSV also includes RHIC data. Hence, the larger gluon uncertainty we find for the `NNPDFpolEIC-B` fit in comparison to Ref. [19] is

likely to be due to our more flexible PDF parametrization, though some difference might also come from the fact that the SIDIS pseudodata included in Ref. [19] provide additional information on the gluon through scaling violations of the fragmentation structure function g_1^h (of course this also introduces an uncertainty related to the fragmentation functions which is difficult to quantify).

In summary, the EIC data would entail a very considerable reduction in the uncertainty on the polarized gluon. They would provide first evidence for a possible nontrivial x shape of the polarized gluon distribution. They would also provide evidence for or against a possible large gluon contribution to the nucleon spin, though the latter goal would still be reached with a sizable residual uncertainty. Additional measurements at an EIC, such as the charm polarized structure function, g_1^c, might provide more information on Δg and its first moment.

Acknowledgements

References

[1] D. de Florian, et al., Phys. Rev. D 80 (2009) 034030, arXiv:0904.3821.
[2] E. Leader, A.V. Sidorov, D.B. Stamenov, Phys. Rev. D 82 (2010) 114018, arXiv:1010.0574.
[3] M. Hirai, S. Kumano, Nucl. Phys. B 813 (2009) 106, arXiv:0808.0413.
[4] J. Blumlein, H. Bottcher, Nucl. Phys. B 841 (2010) 205, arXiv:1005.3113.
[5] NNPDF Collaboration, R.D. Ball, et al., Nucl. Phys. B 874 (2013) 36, arXiv:1303.7236.
[6] D. de Florian, et al., Prog. Part. Nucl. Phys. 67 (2012) 251, arXiv:1112.0904.
[7] COMPASS Collaboration, C. Adolph, et al., Phys. Rev. D 87 (2013) 052018, arXiv:1211.6849.
[8] E.R. Nocera, arXiv:1307.0146, 2013.
[9] PHENIX Collaboration, A. Adare, et al., Phys. Rev. D 79 (2009) 012003, arXiv:0810.0701.
[10] STAR Collaboration, L. Adamczyk, et al., Phys. Rev. D 86 (2012) 032006, arXiv:1205.2735.
[11] STAR Collaboration, L. Adamczyk, et al., arXiv:1309.1800, 2013.
[12] PHENIX Collaboration, A. Adare, et al., Phys. Rev. Lett. 103 (2009) 012003, arXiv:0810.0694.
[13] PHENIX Collaboration, A. Adare, et al., Phys. Rev. D 84 (2011) 012006, arXiv:1009.4921.
[14] A. Deshpande, et al., Annu. Rev. Nucl. Part. Sci. 55 (2005) 165, arXiv:hep-ph/0506148.
[15] D. Boer, et al., arXiv:1108.1713, 2011.

[16] A. Accardi, et al., arXiv:1212.1701, 2012.
[17] H1 Collaboration, ZEUS Collaboration, F. Aaron, et al., J. High Energy Phys. 1001 (2010) 109, arXiv:0911.0884.
[18] LHeC Study Group, J. Abelleira Fernandez, et al., J. Phys. G 39 (2012) 075001, arXiv:1206.2913.
[19] E.C. Aschenauer, R. Sassot, M. Stratmann, Phys. Rev. D 86 (2012) 054020, arXiv:1206.6014.
[20] E.C. Aschenauer, et al., arXiv:1309.5327, 2013.
[21] See for example https://wiki.bnl.gov/eic/.
[22] See for example http://www.jlab.org/elic/.
[23] L. Mankiewicz, A. Schafer, M. Veltri, Comput. Phys. Commun. 71 (1992) 305.
[24] A. Martin, et al., Eur. Phys. J. C 28 (2003) 455, arXiv:hep-ph/0211080.
[25] NNPDF Collaboration, R.D. Ball, et al., Nucl. Phys. B 809 (2009) 1, arXiv:0808.1231.
[26] NNPDF Collaboration, R.D. Ball, et al., Nucl. Phys. B 838 (2010) 136, arXiv:1002.4407.
[27] NNPDF Collaboration, R.D. Ball, et al., Nucl. Phys. B 867 (2013) 244, arXiv:1207.1303.
[28] J. Pumplin, et al., J. High Energy Phys. 0207 (2002) 012, arXiv:hep-ph/0201195.
[29] E. Aschenauer, et al., arXiv:1304.0079, 2013.